PAPER

High-load nanoparticles with a chemotherapeutic SN-38/FdUMP drug cocktail†

Kristina Sabljo,[a] Myrto Ischyropoulou,[b] Joanna Napp,[b] Frauke Alves[b,c,d] and Claus Feldmann [*a]

$[Gd(OH)]^{2+}[(SN-38)_{0.5}(FdUMP)_{0.5}]^{2-}$ inorganic–organic hybrid nanoparticles (IOH-NPs) with a chemotherapeutic cocktail of ethyl-10-hydroxycamptothecin (SN-38, active form of irinotecan) and 5-fluoro-2′-deoxyuridine-5′-phosphate (FdUMP, active form of 5′-fluoruracil), 40 nm in size, are prepared in water. The IOH-NPs contain a total drug load of 63 wt% with 33 wt% of SN-38 and 30 wt% of FdUMP. Cell-based assays show efficient cellular uptake and promising anti-tumour activity on two pancreatic cancer cell lines of murine origin (KPC, Panc02). Beside the high-load drug cocktail, especially the option to use SN-38, which – although 100- to 1000-times more potent than irinotecan – is usually unsuitable for systemic administration due to poor solubility, low stability, and high toxicity upon non-selective delivery. The $[Gd(OH)]^{2+}[(SN-38)_{0.5}(FdUMP)_{0.5}]^{2-}$ IOH-NPs are a new concept to deliver a drug cocktail with SN-38 and FdUMP directly to the tumour, shielded in a nanoparticle, to reduce side effects.

Introduction

Nanoparticles are already the base for many new concepts and materials for cancer treatment and specifically for drug delivery.[1] Such drug-loaded nanoparticles can have essential advantages over the respective free drug in solution. Firstly, nanoparticles allow restricting the widespread distribution of drugs through the body and provide an opportunity for selective delivery exclusively to the site of the tumour. This not only enhances the local activity but also concurrently minimizes undesired side effects on the entire body. Enhanced accumulation at the tumour can be achieved, *e.g.*, *via* the enhanced permeability and retention (EPR) effect and/or by targeting promoted by antibody functionalization.[1,2] As the cell uptake of nanoparticles (*e.g.*, phagocytosis, endocytosis) is different from free drugs (*e.g.*, passive diffusion, ion channels, drug transporters),[3] moreover, nanoparticles can lead to a drug accumulation in or near to the tumor.[4] Here, they can also serve as a drug depot, prolonging the local activity.[3] Finally, the monitoring of nanoparticles in cells, tissue, organs, or whole body is easier in comparison to free drugs due to their larger volume and mass, giving the possibility of multimodal imaging by fluorescent, radiological, and metallic labelling (*e.g.*, *via* optical imaging, magnetic resonance imaging, computed tomography, positron emission tomography).[5] Some drug-loaded nanoparticles were already approved for clinical application. This includes, for instance, non-PEGylated liposomal doxorubicin (Myocet®) or PEGylated liposomal doxorubicin (Caelyx®, Doxil®).[6]

Despite the great potential of drug-loaded nanoparticles, there are still several disadvantages and restrictions for tumour treatment. To avoid uncontrolled leakage and drug release during the delivery to the tumour site, the chemotherapeutic agent is usually encapsulated in certain matrix material such as an organic polymer (*e.g.* polyethylene glycol/PEG) or biopolymer (*e.g.*, polysaccharides, polypeptides),[7] liposomes or micelles,[8] or an inorganic material (*e.g.*, silica, iron oxides, metal phosphates).[9] As a result, the drug load in relation to the total nanoparticle mass is often low (<20%). Although not being a drug, the matrix material can nevertheless cause toxic or allergic effects and needs to be biocompatible for complete removal from the body. Furthermore, high material complexity, limited cell uptake, damage of cell membranes, and/or unexpected toxicity can occur on the long-term.[3,10] Finally, nanoparticles usually only contain a single drug, whereas standard clinical therapy involves drug cocktails of at least two or even more drugs (*e.g.* FOLFIRINOX with folinic acid, 5′-fluorouracil, irinotecan, and oxaliplatin).[11] Such chemotherapeutic

*a*Karlsruhe Institute of Technology (KIT), Institute for Inorganic Chemistry, Engesserstrasse 15, 76131 Karlsruhe, Germany. E-mail: claus.feldmann@kit.edu
*b*University Medical Center Goettingen (UMG), Institute for Diagnostic and Interventional Radiology, Robert Koch Str. 40, 37075 Goettingen, Germany
*c*Max Planck Institute for Multidisciplinary Sciences, Translational Molecular Imaging, Hermann-Rein-Strasse 3, 37075 Goettingen, Germany
*d*University Medical Center Goettingen (UMG), Clinic for Haematology and Medical Oncology, Robert Koch Str. 40, 37075 Goettingen, Germany

cocktails are not only highly effective due to their synergistic, additive and potentiation effects. Yet, they also play a crucial role in overcoming resistances by leveraging drugs with distinct mechanisms of action.[12]

Aiming at a drug-load per nanoparticle as high as possible, we have developed the concept of inorganic–organic hybrid nanoparticles (IOH-NPs).[13] IOH-NPs are characterized by a saline composition with an inorganic cation and a drug anion, which is functionalized by phosphate, sulfonate or carboxylate groups. A recent example is $[ZrO]^{2+}[GMP]^{2-}$ containing gemcitabine phosphate ($[GMP]^{2-}$) as the drug anion with 76% of the total IOH-NP mass and zirconyl ($[ZrO]^{2+}$) as inorganic cation.[14] $[ZrO]^{2+}[GMP]^{2-}$ IOH-NPs turned out to be very promising to treat pancreatic cancer with considerable advantages such as high and selective uptake, low side effects, circumvention of resistances and high activity. Despite of the characteristic high drug load, IOH-NPs nevertheless only contain a single drug. Aiming at high-load chemotherapeutic cocktails, we here focus on the synergistic drug combination with irinotecan (ITC) and 5-fluorouracil (5-FU), which – in combination – are a standard in clinical chemotherapy of pancreatic cancer or colon cancer. Based on the IOH-NP concept, for the first time, we can now realize $[Gd(OH)]^{2+}[(SN\text{-}38)_{0.5}(FdUMP)_{0.5}]^{2-}$ IOH-NPs, which combine SN-38 (100- to 1000-times more active form of ITC) with FdUMP (as a derivative of 5-FU) to a total drug load of 63% per nanoparticle mass.

Experimental section

Synthesis

$[Gd(OH)]^{2+}[(SN\text{-}38)_{0.5}(FdUMP)_{0.5}]^{2-}$ IOH-NPs. 5.6 mg (15 μmol) of SN-38 (99.8%, MedChemExpress, Germany) were dissolved in 12.5 mL of demineralized water and adjusted to pH = 8 by addition of view drops of 0.1 M NaOH to convert the insoluble lactone form to the anionic carboxylate form. In addition, 15.7 mg (45 μmol) of $Na_2(FdUMP)$ (~85%, Sigma Aldrich, Germany) were added. The nucleation of the IOH-NP was induced by injection of an aqueous solution of 15.7 mg (45 μmol) of $GdCl_3 \cdot 8H_2O$ (99.9%, Sigma Aldrich, Germany) in 0.5 mL of demineralized water. The immediate formation of nanoparticles was indicated by the transformation of a yellow solution into a yellow suspension. After two minutes of intense stirring, the as-prepared IOH-NPs were separated from the suspension *via* centrifugation (15 min, 25 000 rpm) and purified twice by redispersion/centrifugation in/from 5 mL of H_2O at pH = 7. Finally, the as-prepared yellowish $[Gd(OH)]^{2+}[(SN\text{-}38)_{0.5}(FdUMP)_{0.5}]^{2-}$ IOH-NPs were dispersed in 5 mL of H_2O (pH = 7), or they were dried in vacuum at room temperature (RT) to obtain powder samples.

$[Gd(OH)]^{2+}[(SN\text{-}38)_{0.5}(UMP)_{0.5}]^{2-}$ IOH-NPs (negative reference). 11.7 mg (0.03 mmol, 99.8%, MedChemExpress) were dissolved in 25 mL of demineralized water and adjusted to pH = 8 by addition of view drops of 0.1 M NaOH. In addition, 33.1 mg (0.09 mmol) of $Na_2(UMP)$ (99%, Alfa Aeasar, USA) were added. The nucleation of the IOH-NPs was induced by

injection of an aqueous solution of 33.5 mg (0.09 mmol, 99.9%, Sigma Aldrich, Germany) in 0.5 mL of demineralized water. After two minutes of intense stirring, the as-prepared IOH-NPs were separated from the suspension *via* centrifugation (15 min, 25 000 rpm) and purified twice by redispersion/centrifugation in/from 5 mL of H_2O at pH = 7. Finally, the as-prepared yellowish $[Gd(OH)]^{2+}[(SN\text{-}38)_{0.5}(UMP)_{0.5}]^{2-}$ IOH-NPs were dispersed in 5 mL of H_2O (pH = 7), or they were dried in vacuum at room temperature to obtain powder samples.

Analytical techniques

Details regarding analytical equipment and IOH-NP characterization are described in the ESI.†

In vitro studies

Cell culture. The Panc02 murine pancreatic ductal adenocarcinoma (PDAC) cell line, derived from C57BL/6 mice after chemical induction of pancreatic tumor[15] and the KPC PDAC cell line (KPCbl6, clone 2.2), established from the primary pancreatic tumour of the genetically engineered KPC mouse model were used.[16]

Panc02 cells were kindly provided by Prof. Stine Falsig Pedersen (Section for Cell Biology and Physiology, Department of Biology, Faculty of Science, University of Copenhagen, Denmark).

KPC cells by Prof. Volker Ellenrieder (Clinic for Gastroenterology, Gastrointestinal Oncology and Endocrinology, University Medical Center Göttingen, Germany).

Panc02 cells were grown in DMEM medium supplemented with 10% fetal bovine serum (FBS, sodium pyruvate, L-glutamine, D-glucose (Gibco) and KPC cells in 10% FBS, 1% NEAA (non-essential amino acids), sodium pyruvate, L-glutamine, and D-glucose (Gibco)). Cells were cultivated at 37 °C with humidified atmosphere of 5% CO_2.

To study the IOH-NP uptake, Panc02 and KPC cells with 13.000 cells per cm^2 were plated on coverslips and incubated for different times (30 min, 5 h, 24 h and 48 h) with 12.5 ng mL^{-1} of $[Gd(OH)]^{2+}[UMP]^{2-}$ IOH-NPs (drug-free reference). After the incubation, the coverslips were washed twice with phosphate-buffered saline (PBS), fixed with 4% paraformaldehyde (PFA) for 10 min at RT and counterstained and mounted with DAPI (1 : 1000, Thermo Fisher Scientific, Germany).

To study anti-tumour efficacy of the IOH-NPs, Panc02 or KPC cells were plated in a 96-well plate at a concentration of 15 000 cells per cm^2 and allowed to attach for 4 h. Afterwards, the cells were treated with gradient concentrations of $[Gd(OH)]^{2+}[(SN\text{-}38)_{0.5}(FdUMP)_{0.5}]^{2-}$ and $[Gd(OH)]^{2+}[(SN\text{-}38)_{0.5}(UMP)_{0.5}]^{2-}$ IOH-NPs, calculated to contain the defined increasing amount of SN-38 (10 nM–2000 nM). Controls included corresponding concentration of $[Gd(OH)]^{2+}[UMP]^{2-}$ IOH-NPs (negative reference) as well as gradient of the freely soluble drug SN-38 (10 nM–2000 nM), either alone or in combination with FdUMP (as contained in the $[Gd(OH)]^{2+}[(SN\text{-}38)_{0.5}(FdUMP)_{0.5}]^{2-}$ IOH-NPs). Due to its solubility

issues, free SN-38 was applied in 0.5% DMSO. Cell confluence was monitored for up to two weeks, using the live cell imaging system (Incucyte^R ZOOM; Sartorius). A two-weeks period ensured that the growth of the tumour cells in response to the respective treatment was adequately monitored without missing potential longer-term effects. Phase-contrast images (2-images per well) were acquired every hour using a 10× objective. The confluence was measured for the individual images by applying confluence mask with the Live-Cell Imaging and Analysis Software (Sartorius). Since untreated control cells reached 100% confluence after approximately three days, a time point of 72 h was selected to calculate the concentration-dependent efficacy (IC$_{50}$ values).

Microscopy and image analysis. A Leica SP5 confocal laser scanning microscope was used for fluorescence imaging, with λ_{Ex} = 549 nm λ_{Em} = 559–650 nm for DUT549-labelled [Gd (OH)]$^{2+}$[UMP]$^{2-}$ IOH-NPs and λ_{Ex} = 405 nm and λ_{Em} = 415–479 nm for DAPI. 0.15 μm Z-stacks were acquired. The images were analysed with Image J.[17]

Statistical analysis. Statistical analyses were performed with GraphPad Prism 9 Software. All diagrams show mean values with ± SEM.

Results and discussion

Selection of drugs

Irinotecan (ITC) belongs to a class of chemotherapeutic drugs known as topoisomerase I inhibitors and represents a semisynthetic analogue of the natural alkaloid camptothecin.[18] ITC is a prodrug, which needs to be hepatically metabolised to SN-38 (7-ethyl-10-hydroxycamptothecin) as the active drug. This conversion of ITC to SN-38 involves hydrolysis, catalysed by carboxylesterases (CES) in the liver, which, however, is with low efficiency (2–8% *in vivo*). The then formed SN-38 has a considerably greater potency (up to 1000-times) than ITC.[19] Beside lower potency and need of conversion in the liver, ITC also shows disadvantages during body clearance. After formation in the liver, SN-38 is partially excreted into the intestinal lumen through bile after conjugation to SN-38 glucuronide (SN-38G) by hepatic uridine diphosphate glucuronosyl transferase. Once in the intestinal lumen, SN-38G undergoes substantial deconjugation by bacterial beta-glucuronidase, resulting in a reformation of SN-38. This regeneration of SN-38 within the intestinal lumen triggers severe gastrointestinal reactions such as diarrhea, nausea, bloody stools, and/or colon inflammation. Despite these disadvantages, the pro-drug ITC is widely used in the clinics and very effective against numerous malignant tumors (including lung, colorectal, gastric, lymph, cervical, ovarian cancers). In contrast, a direct application of the active drug SN-38 is normally excluded due to its poor water solubility (11 μg mL^{-1}), its low stability in physiological media, and its high potency causing severe side effects if non-selectively distributed over the whole body.[20]

5-Fluorouracil (5-FU) is one of the most relevant chemotherapeutic agents, again including lung, colorectal, gastric, lymph, cervical, and ovarian cancers. It directly acts on the DNA synthesis by blocking the thymidylate synthase and is applied in its active form.[21] 5-FU is one of the oldest chemotherapeutic agents with well-defined treatment regimens. Although allowing an effective treatment for various types of cancer, 5-FU still has several drawbacks that limit its clinical use and may have negative impact on the patient's outcome. These include toxicity, drug resistance, non-specific cytotoxicity, variable patient responses, and restrictions regarding administration. 5-FU is not specific to cancer cells and can affect rapidly dividing normal cells, such as those in the gastrointestinal tract, bone marrow, and hair follicles, leading to toxicities like gastrointestinal issues (including nausea, vomiting, diarrhea) as well as cardiotoxicity, myelosuppression, and hand-foot syndrome. Patients on 5-FU also have an increased risk of partially life-threatening side effects, such as severe infections, sepsis, and mucositis. Finally, 5-FU has a relatively short half-life, requiring continuous infusion or frequent dosing to maintain therapeutic levels. These limitations point to the need of developing improved delivery systems (*e.g.*, nanoparticles) and/or alternative therapeutic strategies to improve the safety and efficacy of 5-FU and, in sum, the patient's quality of life.[22]

In sum, a combination of the clinically highly relevant drugs ITC and 5-FU – and even more preferable SN-38 and 5-FU – with high load in a single nanoparticle is extremely attractive as a selective delivery and release could lead to a significantly higher efficacy and/or considerably lower side effects as compared to the current clinical therapy based on freely dissolved drugs. Nanoparticles with high load of both ITC and 5-FU, and especially of SN-38 and 5-FU, however, were not available before.

Nanoparticle synthesis

Based on the IOH-NP concept with phosphate- or carboxylate-functionalized drug anions and a certain inorganic cation to make the IOH-NPs insoluble in water, we used the carboxylate-functionalized SN-38 as the active and much more potent form of ITC (Fig. 1a). Moreover, the phosphate-functionalized 5-fluoro-2′-deoxyuridylate (FdUMP) was used as anionic derivative of 5′-fluoruracil (Fig. 1a). To make both anions [SN-38]$^{2-}$
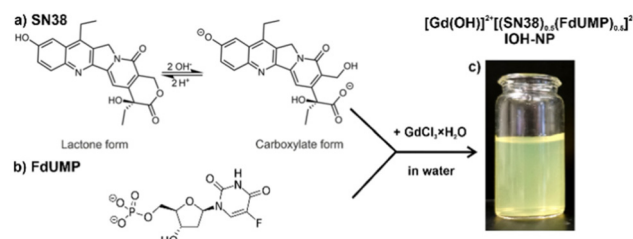

Fig. 1 Scheme illustrating the aqueous synthesis of [Gd (OH)]$^{2+}$[(SN-38)$_{0.5}$(FdUMP)$_{0.5}$]$^{2-}$ IOH-NPs with SN-38 (a) and FdUMP (b) as drug anions as well as a photo of the resulting aqueous suspension (c).[‡]

and $[FdUMP_5]^{2-}$ insoluble in water, $[Gd(OH)]^{2+}$ turned out to be an appropriate inorganic cation.

Following the aqueous synthesis of IOH-NPs,[13,14] a concentrated solution of $GdCl_3 \cdot 8H_2O$ in water was injected with vigorous stirring into a solution of SN-38 and $Na_2(FdUMP)$ in water (Fig. 1b). To do so, first of all, the water-insoluble lactone form of SN-38 needs to be converted into the carboxylate form at slightly alkaline conditions (pH 8) prior to particle nucleation. Upon injection of $GdCl_3 \cdot 8H_2O$ to the solution of the drug anions, immediate nucleation and particle growth occur as indicated by certain turbidity of the liquid phase (Fig. 1c). The as-prepared $[Gd(OH)]^{2+}[(SN-38)_{0.5}(FdUMP)_{0.5}]^{2-}$ IOH-NPs were purified by centrifugation/redispersion in/from water to remove all remaining starting materials and salts. Thereafter, the IOH-NPs were dried to powder samples or redispersed in water to obtain colloidally stable suspensions (Fig. 1c).

Particle size, size distribution and colloidal stability of the as-prepared $[Gd(OH)]^{2+}[(SN-38)_{0.5}(FdUMP)_{0.5}]^{2-}$ IOH-NPs were characterized by dynamic light scattering (DLS) and scanning electron microscopy (SEM). DLS of aqueous suspensions indicates a mean hydrodynamic diameter of 66 ± 16 nm (Fig. 2a). SEM confirms the presence of spherical particles with a mean diameter of 38 ± 7 nm (based on statistical evaluation of >100 nanoparticles on SEM images) (Fig. 2a and b). Such particle size is considered as optimal for biomedical application as the particles are large enough to avoid immediate renal clearance (>20 nm) but to also avoid embolism (<100 nm). The larger diameter from DLS compared to the value obtained by SEM relates to the hydrodynamic diameter and a rigid layer of water molecules adsorbed on the particle surface. Aqueous IOH-NP suspensions are colloidally highly stable without the need of any additional surface-active agent. They do not show any sedimentation over 3–4 weeks. The high colloidal stability can be ascribed to the intrinsic charge stabilization of the IOH-NPs. Thus, zeta-potential measurements prove negative charging of −10 to −30 mV in the physiologically most relevant pH range of 6.5–7.5 (Fig. 2c).

Composition and fluorescence

The chemical composition and drug load of the $[Gd(OH)]^{2+}[(SN-38)_{0.5}(FdUMP)_{0.5}]^{2-}$ IOH-NPs was evaluated with different analytical methods. In regard of the high costs of FdUMP (*i.e.* about 4000 € for 100 mg $Na_2(FdUMP)$), we have performed the chemical characterization with $[Gd(OH)]^{2+}[(SN-38)_{0.5}(UMP)_{0.5}]^{2-}$ (*i.e.* about 5 € for 100 mg $Na_2(UMP)$). In difference to FdUMP, UMP does not contain any fluorine and, therefore, is not cytotoxic, which, however, does not affect the particle size or overall composition of the IOH-NPs (except for the absence of fluorine).

According to X-ray powder diffraction (XRD), the IOH-NPs are amorphous. This finding is not a surprise taking the low temperature of synthesis and the large volume of the drug anions into account. In fact, amorphous drug nanocarriers are often advantageous in regard of their dissolution kinetics,[23] which is slow enough to achieve maintenance of high tumour concentrations but rapid enough to avoid side effects due to particle accumulation. Qualitatively, Fourier-transform infrared (FT-IR) spectroscopy evidences the presence of the respective drug anions (Fig. 2d). Thus, the characteristic vibrations of SN-38 ($\nu(R-COO)$: 1585 cm^{-1}) and UMP (or FdUMP) ($\nu(C=O)$: 1680 cm^{-1}, $\nu(P-O)$: 1100–970 cm^{-1}) are clearly observed. These vibrations are well in agreement with the starting materials as references. Energy dispersive X-ray spectroscopy (EDXS) confirms the presence of gadolinium and phosphorus in the IOH-NPs (ESI: Fig. S1†). Finally, the chemical composition of the IOH-NPs was quantified by total organics combustion *via* elemental analysis (EA) and thermogravimetry (TG). As a result, the IOH-NPs contain 33 wt% of SN-38 and 30 wt% of UMP (or FdUMP) (Table 1 and ESI: Fig. S2†). This confirms the intended 1:1 ratio of SN-38 and FdUMP in the IOH-NPs. Moreover, the good coincidence of the experimental and the calculated data evidences the overall composition $[Gd(OH)]^{2+}[(SN-38)_{0.5}(FdUMP)_{0.5}]^{2-}$ with a total drug load of 63 wt% (remaining 37 wt% due to inorganic $[Gd(OH)]^{2+}$ cation).

Beside the above analytical characterization, specifically the presence of SN-38 can be also validated by optical spectroscopy (UV-Vis). Thus, the characteristic absorption below 450 nm is observed for the IOH-NPs as well as for alkaline solutions of
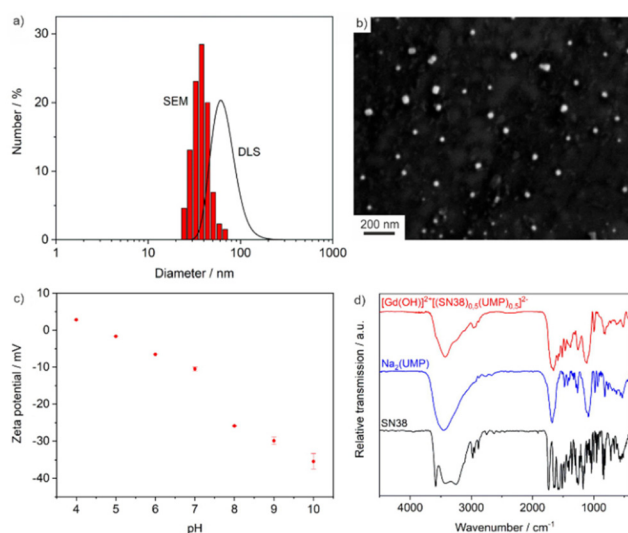

Fig. 2 Particle features of $[Gd(OH)]^{2+}[(SN-38)_{0.5}(FdUMP)_{0.5}]^{2-}$ IOH-NPs: (a) size and size distribution according to DLS (in water) and SEM; (b) SEM overview image; (c) zeta potential of aqueous suspension; (d) FT-IR spectra ($Na_2(UMP)$ and SN-38 as references).

Table 1 Composition of $[Gd(OH)]^{2+}[(SN-38)_{0.5}(UMP)_{0.5}]^{2-}$ IOH-NPs according to elemental analysis (EA) and thermogravimetry (TG)

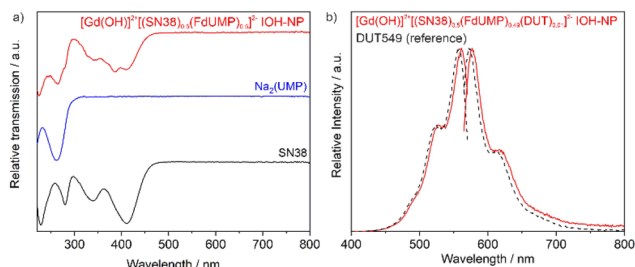|	EA contents			
	N/wt%	C/wt%	H/wt%	TG mass loss/wt%
Experimental	5.0	32.5	3.2	64.9
Calculated	5.2	34.4	3.1	65.2

Fig. 3 Optical properties of $[Gd(OH)]^{2+}[(SN-38)_{0.5}(UMP)_{0.5}]^{2-}$ IOH-NPs: (a) UV-Vis spectrum (with $Na_2(UMP)$ and alkaline SN-38 solution as references); (b) fluorescence spectra of DUT549-labelled IOH-NPs (λ_{ex} = 550 nm, λ_{em} = 585 nm; free DUT549 as a reference).

SN-38 (pH = 8) (Fig. 3a). Furthermore, the absorptions at 335 and 410 nm are characteristic for the open carboxylate form of SN-38 (ESI: Table S1 and Fig. S3–S8†). These absorptions are also in accordance with the yellowish colour of the $[Gd(OH)]^{2+}[SN-38]^{2-}$ IOH-NPs and alkaline solutions of SN-38 (Fig. 1).

To enable the $[Gd(OH)]^{2+}[(SN-38)_{0.5}(FdUMP)_{0.5}]^{2-}$ IOH-NPs for fluorescence-based monitoring, they were labelled with minor amounts (0.01 mol%) of Dyomics DY-549-dUTP (DUT549) as a fluorescent dye (Fig. 3b). DUT549 shows red emission at 570–700 nm (λ_{max} = 585 nm) upon excitation at 460–570 nm. Similar to FdUMP, DUT549 is phosphate-functionalized and can be easily incorporated in the IOH-NPs upon addition together with FdUMP. Moreover, it should be noticed that SN-38 shows emission itself with greenish emission (500–650 nm, λ_{max} = 560 nm) upon excitation at 400–500 nm (ESI: Fig. S9†). Although we did not use the SN-38-based emission, it is an additional option for optical imaging.

In vitro studies

To assess the chemotherapeutic effectiveness of the $[Gd(OH)]^{2+}[(SN-38)_{0.5}(FdUMP)_{0.5}]^{2-}$ IOH-NPs, it is crucial to ensure their successful uptake by the tumour cells. Therefore, the cellular internalization of the IOH-NPs was examined in two different pancreatic ductal adenocarcinoma (PDAC) cell lines of murine origin (KPC, Panc02), using confocal microscopy (Fig. 4). To safeguard against premature cell death during uptake studies, the cells were incubated with drug-free $[Gd(OH)]^{2+}[UMP]^{2-}$ IOH-NPs. These reference IOH-NPs exclusively contain the non-toxic uridine monophosphate (UMP) but neither SN-38 nor FdUMP. Similar to the drug-loaded IOH-NPs, these reference IOH-NPs were labelled with DUT549 as a fluorescent dye.

To accommodate the genetic diversity observed in PDAC, both mouse pancreatic cancer cell lines – KPC and Panc02 – were exposed to drug-free reference $[Gd(OH)]^{2+}[UMP]^{2-}$ IOH-NPs at a concentration of 12.5 ng mL^{-1}. Subsequently, the cellular uptake was tracked using confocal microscopy after 0.5, 5, 24 and 48 h of incubation. The DUT549-labeled $[Gd(OH)]^{2+}[UMP]^{2-}$ IOH-NPs exhibit a distinctive intense red fluorescence (Fig. 4). Cell nuclei were counterstained with 4′,6-di-

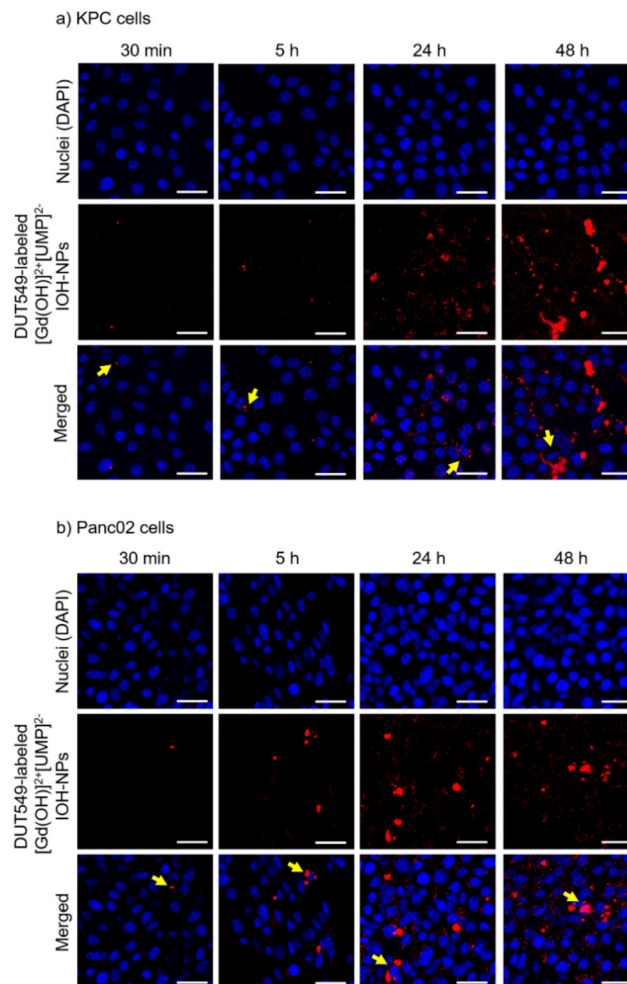**Fig. 4** Cell uptake of DUT549-labeled reference $[Gd(OH)]^{2+}[UMP]^{2-}$ IOH-NPs in (a) KPC and (b) Panc02 PDAC cells, monitored with confocal fluorescence microscopy over time (after 0.5, 5, 24 and 48 h of incubation at 37 °C). DUT549-labeled IOH-NPs were imaged with λ_{ex} = 549 nm, λ_{em} = 559–650 nm (red); DAPI staining with λ_{ex} = 405 nm, λ_{em} = 415–479 nm (blue). Yellow arrows on merged images point to the cells, which have taken up extraordinary high amounts of IOH-NPs. Scale bar corresponds to 25 μm in all images.

amidino-2-phenylindole (DAPI) displaying blue emission. A time-dependent increase in the nanoparticle uptake was clearly observed as indicated by the emission of red light, resulting in a substantial load of the IOH-NPs within both pancreatic cancer cell lines after 48 h of incubation. In Panc02 cells, the cellular uptake of the IOH-NPs was visible already after 5 h (Fig. 4a), whereas an uptake by KPC cells was first detectable after 24 h (Fig. 4b). The IOH-NPs can be assumed to follow the endocytic pathways for cell internalization, before they reach acidic compartments for dissolution. Such mechanism is known for a variety of nanocarriers[24] and is also in accordance with our previous findings, showing IOH-NPs to end up in late endosomes and lysosomes of human PDAC cells after internalization.[14,25] Notably, the IOH-NPs exhibit specific accumulation in the vicinity of the cell nuclei, which is advan-

tageous as the IOH-NP dissolution and the release of SN-38 and FdUMP are close to the nucleus as the site of action.

PDAC tumours are characterized by a considerably increased probability of genetic mutations, leading to an increased genetic variability within the cells.[26] These mutations can pose a significant challenge in achieving an effective treatment due to their impact on the cell susceptibility to various drugs. Consequently, two different PDAC murine cell lines – KPC cells (with p53 and KRAS mutation, Fig. 5) and Panc02 (with SMAD4 mutation, Fig. 6) were applied to assess the efficacy of the $[Gd(OH)]^{2+}[(SN-38)_{0.5}(FdUMP)_{0.5}]^{2-}$ IOH-NPs with two drugs, $[Gd(OH)]^{2+}[(SN-38)_{0.5}(UMP)_{0.5}]^{2-}$ IOH-NPs with only one drug as well as the free drugs SN-38 alone or SN-38 + FdUMP (positive controls) and the drug-free $[Gd(OH)]^{2+}[UMP]^{2-}$ IOH-NPs (negative control). Live-cell imaging was employed for up to 2 weeks to monitor the confluence hourly, utilising phase-contrast microscopy and a predefined cell-identification mask (Fig. 5 and 6). Such an extended time has been selected to observe not only short-term cytotoxicity but also any delayed responses to the IOH-NPs treatment and to assess the long-term viability of the remaining cells and any potential recovery or regrowth. IOH-NPs toxicity has been observed as early as after 1–2 days of incubation, with no hints for the delayed effects within the experimental setting. Since the untreated control cells reached confluence after approximately three days, a time point of 72 h was selected to calculate the concentration-dependent efficacy (Table 2).

In general, the drug-loaded IOH-NPs demonstrate a notable anti-tumour efficacy in both PDAC cell lines, confirming not only an efficient uptake of the IOH-NPs but also an effective
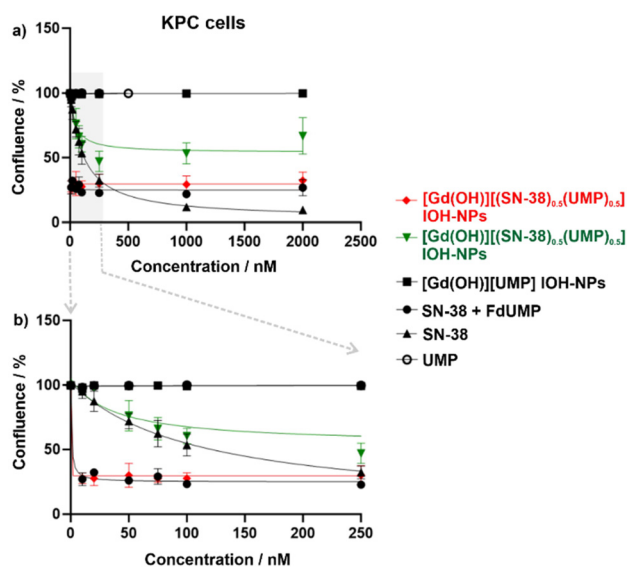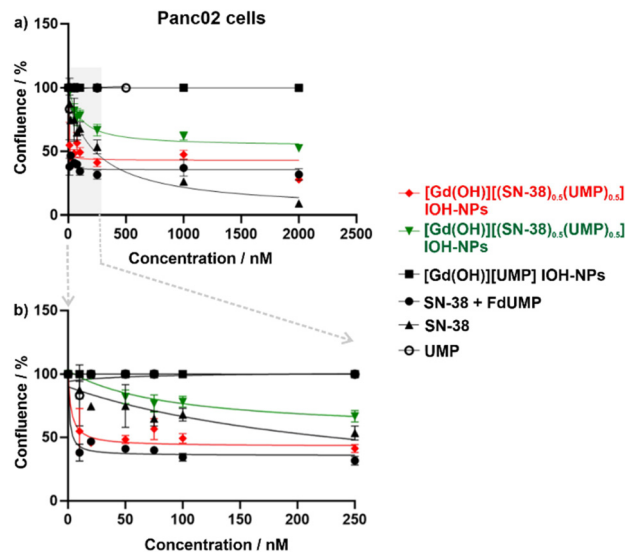

Fig. 6 Confluence of Panc02 cells monitored *via* live-cell imaging the response of gradient concentrations of 10–2000 nM (a) and enlarged of 10–250 nM (b) of $[Gd(OH)]^{2+}[(SN-38)_{0.5}(FdUMP)_{0.5}]^{2-}$ IOH-NPs, $[Gd(OH)]^{2+}[(SN-38)_{0.5}(UMP)_{0.5}]^{2-}$ IOH-NPs and $[Gd(OH)]^{2+}[UMP]^{2-}$ IOH-NPs as well as the freely dissolved drugs SN-38 + FdUMP and SN-38 after 72 hours of treatment.

Table 2 IC_{50} of the IOH-NPs in comparison with the values of their soluble free drugs alone or in combination determined after 72 hours of treatment

	Drugs	Panc02 cells	KPC cells
Nanoparticles			
$[Gd(OH)]^{2+}[(SN-38)_{0.5}(FdUMP)_{0.5}]^{2-}$	SN-38, FdUMP	43.4 ± 31.2 nM	11.0 ± 2.2 nM
$[Gd(OH)]^{2+}[(SN-38)_{0.5}(UMP)_{0.5}]^{2-}$	SN-38	247.5 ± 31.8 nM	198.9 ± 80.5 nM
$[Gd(OH)]^{2+}[UMP]^{2-}$	None	No toxicity	No toxicity
Free drugs			
SN-38 + FdUMP	SN-38, FdUMP	28.5 ± 2.7 nM	6.9 ± 3.2 nM
SN-38	SN-38	159.3 ± 53 nM	98.6 ± 34.9 nM

Fig. 5 Confluence of KPC cells monitored *via* live-cell imaging to assess the response of gradient concentrations of 10–2000 nM (a) and enlarged of 10–250 nM (b) of $[Gd(OH)]^{2+}[(SN-38)_{0.5}(FdUMP)_{0.5}]^{2-}$ IOH-NPs, $[Gd(OH)]^{2+}[(SN-38)_{0.5}(UMP)_{0.5}]^{2-}$ IOH-NPs and $[Gd(OH)]^{2+}[UMP]^{2-}$ IOH-NPs as well as the freely dissolved drugs SN-38 + FdUMP and SN-38 after 72 hours of treatment.

release of the active drugs from the nanoparticles. $[Gd(OH)]^{2+}[(SN-38)_{0.5}(UMP)_{0.5}]^{2-}$ IOH-NPs show a mean inhibitory concentration (IC_{50}), representing the concentration required to reduce confluence to 50% of the initial value, of 247.5 ± 31.8 nM in Panc02 cells and 198.9 ± 80.5 nM in KPC cells (Table 2). $[Gd(OH)]^{2+}[(SN-38)_{0.5}(FdUMP)_{0.5}]^{2-}$ IOH-NPs exhibit an even higher effectiveness with 5–10-fold lower IC_{50} values of 43.4 ± 31.2 nM in Panc02 and 11.0 ± 2.2 nM in KPC cells. This reinforces the synergistic effect of the drug cocktail in the $[Gd(OH)]^{2+}[(SN-38)_{0.5}(FdUMP)_{0.5}]^{2-}$ IOH-NPs. Interestingly, KPC cells were more responsive than Panc02 cells (Fig. 5 and 6), not only to the IOH-NPs but also to both soluble drugs. This could possibly be attributed to the faster doubling time of KPC cells, as chemotherapeutic agents are known to affect rapidly dividing cells more significantly, with less impact on slow-proliferating cells.[27] Additionally, the two cell lines carry

different genetic mutations, which could potentially influence their susceptibility to the selected drugs.

While both single- and double-drug-loaded IOH-NPs show impressive efficacy on the tested PDAC cells, the efficacy of the free drugs in solution – *i.e.*, SN-38 and SN-38 + FdUMP – is still slightly higher (Fig. 5 and 6). This is to be expected and can be attributed to the immediate availability of the freely dissolved chemotherapeutics when applied directly to the cell-culture medium, whereas the IOH-NPs, first, require cell uptake, followed by endosomal trafficking,[14,25] and only thereafter the release of the active drug to achieve cytotoxic effects. Even more important, it has to be taken into account that SN-38, though highly potent when applied *in vitro* to cultured cells, exhibits limited efficacy when applied systemically *in vivo* due to stability issues, thus, making it yet unsuitable for systemic administration.[28] Current nanoparticle concepts failed so far for several reasons, such as insufficient stability and/or insufficient SN-38 load (<3 wt%).[29] $[Gd(OH)]^{2+}[(SN-38)_{0.5}(FdUMP)_{0.5}]^{2-}$ IOH-NPs, however, could open the option of using the 100- to 1000-times more potent SN-38, while minimizing the issues associated with a direct SN-38 administration (*i.e.*, low solubility, poor stability, severe side-effects for uncontrolled distribution).

Conclusions and outlook

In conclusion, the newly presented $[Gd(OH)]^{2+}[(SN-38)_{0.5}(UMP)_{0.5}]^{2-}$ and $[Gd(OH)]^{2+}[(SN-38)_{0.5}(FdUMP)_{0.5}]^{2-}$ IOH-NPs introduce a novel highly promising nanocarrier system to deliver SN-38 either alone or in conjunction with 5-FU, which provides a whole range of advantages. With a total drug load of 63% – thereof 33 wt% of SN-38 and 30 wt% of FdUMP – they contain a drug cocktail of clinically highly relevant chemotherapeutic agents with an exceptional load. Due to dye labelling, the IOH-NPs can be monitored easily. Cell-based assays show efficient cellular uptake and promising anti-tumour activity on two pancreatic cancer cell lines of murine origin (KPC, Panc02), comparable even to the freely dissolved drugs. The direct delivery of the highly potent SN-38 without relying on the less efficient enzymatic activation of irinotecan as a prodrug in the liver could become most relevant for clinical therapy. SN-38 can be protected in the nanoparticle and delivered to the tumour (*e.g.* after intravenous administration), where it develops its high efficacy but causing less of the severe side effects (*e.g.*, diarrhea, bone-marrow toxicities, colon inflammation). Beside the high load of a chemotherapeutic cocktail, in sum, direct delivery of SN-38 in form of IOH-NPs may not only eliminate the severe adverse reactions, but also further enhance curative effects without the need for increased dosage, addressing issues related to solubility and stability without compromising its activity.

Data availability

Additional data regarding experiments and methods can be obtained from the ESI† and on request from the authors.

Conflicts of interest

There are no conflicts to declare.

Acknowledgements

References

1 (*a*) P. Grodzinski, M. Kircher, M. Goldberg and A. Gabizon, *ACS Nano*, 2019, **13**, 7370–7376; (*b*) J. Wolfram and M. Ferrari, *Nano Today*, 2019, **25**, 85–98.

2 (*a*) A. C. Marques, P. J. Costa, S. Velho and M. H. Amaral, *J. Controlled Release*, 2020, **320**, 180–200; (*b*) F. M. Kashkooli, M. Soltani and M. Souri, *J. Controlled Release*, 2020, **327**, 316–349.

3 S. Behzadi, V. Serpooshan, W. Tao, M. A. Hamaly, M. Y. Alkawareek, E. C. Dreaden, D. Brown, A. M. Alkilany, O. C. Farokhzad and M. Mahmoudi, *Chem. Soc. Rev.*, 2017, **46**, 4218–4244.

4 (*a*) J. Xiang, Y. Li, Y. Zhang, G. Wang, H. Xu, Z. Zhou, J. Tang and Y. Shen, *J. Controlled Release*, 2021, **330**, 992–1003; (*b*) Y. Li, L. Yang, X. Xu, M. Li, Y. Zhang, Q. Lin, T. Gong, X. Sun, Z. Zhang and L. Zhang, *ACS Appl. Mater. Interfaces*, 2021, **13**, 46361–46374; (*c*) T. Zhao, P. Wang, Q. Li, A. A. Al-Khalaf, W. N. Hozzein, F. Zhang, X. Fan and D. Zhao, *Angew. Chem., Int. Ed.*, 2018, **57**, 2611–2615.

5 (*a*) S. Kunjachan, J. Ehling, G. Storm, F. Kiessling and T. Lammers, *Chem. Rev.*, 2015, **115**, 10907–10937; (*b*) T. L. Doane and C. Burda, *Chem. Soc. Rev.*, 2012, **41**, 2885–2911.

6 (*a*) Y. Barenholz, *J. Controlled Release*, 2012, **160**, 117–134; (*b*) W. J. Gradishar, S. Tjulandin, N. Davidson, H. Shaw, D. Heather, N. Desai, P. Bhar, M. Hawkins and J. O'Shaughnessy, *J. Clin. Oncol.*, 2005, **23**, 7794–7803.

7 (*a*) D. Shi, D. Beasock, A. Fessler, J. Szebeni, J. Y. Ljubimova, K. A. Afonin and M. A. Dobrovolskaia, *Adv. Drug Delivery Rev.*, 2022, **180**, 114079; (*b*) B. Ghosh and S. Biswas, *J. Controlled Release*, 2021, **332**, 127–147; (*c*) S. E. Birk, A. Boisen and K. H. Nielsen, *Adv. Drug Delivery Rev.*, 2021, **174**, 30–52; (*d*) C. D. Spicer, C. Jumeaux, B. Gupta and M. M. Stevens, *Chem. Soc. Rev.*, 2018, **47**, 3574–3620; (*e*) M. Dangol, H. Yang, C. G. Li, S. F. Lahiji, S. Kim, Y. Ma and H. Jung, *J. Controlled Release*, 2016, **223**, 118–125; (*f*) C. E. Wang, P. S. Stayton, S. H. Pun and

A. J. Convertine, *J. Controlled Release*, 2015, **219**, 345–354; (*g*) M. Talelli, M. Barz, C. J. F. Rijcken, F. Kießling, W. E. Hennink and T. Lammers, *Nano Today*, 2015, **10**, 93–117; (*h*) D. Ma, G. Hettiarachchi, D. Nguyen, B. Zhang, J. B. Wittenberg, P. Y. Zavalij, V. Briken and L. Isaacs, *Nat. Chem.*, 2012, **4**, 503–510.

8 (*a*) X.-H. Cao, M.-X. Liang, Y. Wu, K. Yang, J.-H. Tang and W. Zhang, *Nanomedicine*, 2021, **16**, 1519–1537; (*b*) A. A. Aghdam, R. Bagheri, J. Mosafer, B. Baradaran, M. Hashemzaei, A. Baghbanzadeh, M. de la Guardia and A. Mokhtarzadeh, *J. Controlled Release*, 2019, **315**, 1–22; (*c*) X. Liu, F. Wu, Y. Ji and L. Yin, *Bioconjugate Chem.*, 2019, **30**, 305–324; (*d*) H. Cabral and K. Kataoka, *J. Controlled Release*, 2014, **190**, 465–476.

9 (*a*) A. Jozefczak, K. Kaczmarek and R. Bielas, *Theranostics*, 2021, **11**, 10091–10113; (*b*) H. Huang, W. Feng, Y. Chen and J. Shi, *Nano Today*, 2020, **35**, 100972; (*c*) J. Liu, J. Dong, T. Zhang and Q. Peng, *J. Controlled Release*, 2018, **286**, 64–73; (*d*) J.-J. Hu, D. Xiao and X. Z. Zhang, *Small*, 2016, **12**, 3344–3359; (*e*) A. B. Satterlee and L. Huang, *Theranostics*, 2016, **6**, 918–929; (*f*) D. Ling, N. Lee and T. Hyeon, *Acc. Chem. Res.*, 2015, **48**, 1276–1285; (*g*) A. K. Gupta and M. Gupta, *Biomaterials*, 2005, **26**, 3995–4021; (*h*) C. Barbe, J. Bartlett, L. Kong, K. Finnie, H. Q. Lin, M. Larkin, S. Calleja, A. Bush and G. Calleja, *Adv. Mater.*, 2004, **16**, 1959–1966.

10 V. Schirrmacher, *Int. J. Oncol.*, 2019, **54**, 407–419.

11 J. E. Faris, L. S. Blaszkowsky, S. McDermott, A. R. Guimaraes, J. Szymonifka, M. A. Huynh, C. R. Ferrone, J. A. Wargo, J. N. Allen, L. E. Dias, *et al.*, *Oncology*, 2013, **18**, 543–548.

12 W. Fan, B. Yung, P. Huang and X. Chen, *Chem. Rev.*, 2017, **117**, 13566–13638.

13 M. Roming, H. Lünsdorf, K. E. J. Dittmar and C. Feldmann, *Angew. Chem., Int. Ed.*, 2010, **49**, 632–637.

14 M. Ischyropoulou, K. Sabljo, L. Schneider, C. M. Niemeyer, J. Napp, C. Feldmann and F. Alves, *Adv. Mater.*, 2023, 2305151.

15 T. H. Corbett, B. J. Roberts, W. R. Leopold, J. C. Peckham, L. J. Wilkoff and D. P. Griswold, *Cancer Res.*, 1984, **44**, 717–726.

16 J. W. Lee, C. A. Komar, F. Bengsch, K. Graham and G. L. Beatty, *Curr. Protoc. Pharmacol.*, 2016, **73**, 14.39.1–14.39.20.

17 J. Schindelin, I. Arganda-Carreras, E. Frise, V. Kaynig, M. Longair, T. Pietzsch, S. Preibisch, C. Rueden, S. Saalfeld, B. Schmid, *et al.*, *Nat. Methods*, 2012, **9**, 676–682.

18 J. Robert and L. Rivory, *Drugs Today*, 1998, **34**, 777–803.

19 M. Ramesh, P. Ahlawat and N. R. Srinivas, *Biomed. Chromatogr.*, 2010, **24**, 104–123.

20 Z. L. Song, H. L. Chen, Y. H. Wang, M. Goto, W. J. Gao, P. L. Cheng, S. Morris-Natschke, Y. Q. Liu, G. X. Zhu, M. J. Wang and K. H. Lee, *Bioorg. Med. Chem. Lett.*, 2015, **25**, 2690–2693.

21 (*a*) Y. Nakajima, M. Iigo and A. Hoshi, *Anticancer Drugs*, 1992, **3**, 289–292; (*b*) R. L. Drengler, J. G. Kuhn, L. J. Schaaf, G. I. Rodriguez, M. A. Villalona-Calero, L. A. Hammond, J. A. Stephenson, S. Hodges, M. A. Kraynak, B. A. Staton, *et al.*, *J. Clin. Oncol.*, 1999, **17**, 685–696.

22 (*a*) S. Ghafouri-Fard, A. Abak, F. T. Anamag, H. Shoorei, F. Fattahi, S. A. Javadinia, A. Basiri and M. Taheri, *Front. Oncol.*, 2021, **11**, 658636; (*b*) N. Zhang, Y. Yin, S. J. Xu and W. S. Chen, *Molecules*, 2008, **13**, 1551–1569.

23 R. Jog and D. J. Burgess, *J. Pharm. Sci.*, 2017, **106**, 39–65.

24 (*a*) J. J. Rennick, A. P. R. Johnston and R. G. Parton, *Nat. Nanotechnol.*, 2021, **16**, 266–276; (*b*) S. G. Smith, L. I. Selby, A. P. R. Johnston and G. K. Such, *Bioconjugate Chem.*, 2019, **30**, 263–272.

25 (*a*) M. Khorenko, A. Meschkov, J. Napp, J. Pfeifer, J. Stier, F. Alves, U. Schepers and C. Feldmann, *J. Mater. Chem. B*, 2023, **11**, 3635–3649; (*b*) C. Ritschel, J. Napp, F. Alves and C. Feldmann, *Nanoscale*, 2022, **14**, 16249–16255; (*c*) K. Sabljo, J. Napp, F. Alves and C. Feldmann, *Chem. Commun.*, 2022, **58**, 9417–9420.

26 Y. Wang, Y. Zhang, J. Yang, X. Ni, S. Liu, Z. Li, S. E. Hodges, W. E. Fisher, F. C. Brunicardi, R. A. Gibbs, M.-C. Gingras and M. Li, *Curr. Mol. Med.*, 2012, **12**, 331–341.

27 E. Kondoh, S. Mori, K. Yamaguchi, T. Baba, N. Matsumura, J. C. Barnett, R. S. Whitaker, I. Konishi, S. Fujii, A. Berchuck and S. K. Murphy, *Int. J. Cancer*, 2010, **126**, 2448–2456.

28 (*a*) S. Palakurthi, *Expert Opin. Drug Delivery*, 2015, **12**, 1911–1921; (*b*) D. Zheng, Y. Wang, D. Zhang, Z. Liu, C. Duan, L. Jia, F. Wang, Y. Liu, G. Liu, L. Hao and Q. Zhang, *Cancer Lett.*, 2011, **307**, 158–164.

29 (*a*) M. Chen, W. Li, X. Zhang, Y. Dong, Y. Hua, H. Zhang, J. Gao, L. Zhao, Y. Li and A. Zheng, *Int. J. Nanomed.*, 2017, **12**, 5487–5500; (*b*) Y. Matsumura, *Adv. Drug Delivery Rev.*, 2011, **63**, 184–192; (*c*) T. E. Nakajima, M. Yasunaga and Y. Kano, *Int. J. Cancer*, 2008, **122**, 2148–2153; (*d*) M. Sumitomo, F. Koizumi, T. Asano, A. Horiguchi, K. Ito, T. Asano, T. Kakizoe, M. Hayakawa and Y. Matsumura, *Cancer Res.*, 2008, **68**, 1631–1635.